P14.2 INTERPRETATION OF THE "FLYING EAGLE" RADAR SIGNATURE IN SUPERCELLS

MATTHEW R. KUMJIAN* AND ALEXANDER D. SCHENKMAN
School of Meteorology, University of Oklahoma, Norman, OK

1. INTRODUCTION

A common feature of supercells on radar displays is a winged or branched appearance of the reflectivity field in the forward-flank of the storm (Fig. 1). This signature is given a variety of names throughout the community, some of which include: flying eagle, screaming eagle, spread eagle, butterfly, wings, and v-notch. Despite the prevalence of this echo pattern and its recognition amongst many meteorologists, it still generates intrigue and often confusion when it comes to the explanation of its origin. A common explanation circulating in the meteorology community is one that invokes an analogy to obstacle flow, perhaps stemming from early publications. However, more recent research has shown that the updraft is not a solid obstacle and thus the analogy is rather tenuous.

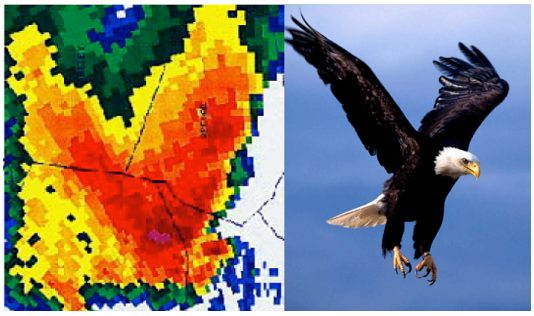

Fig. 1: Reflectivity field of a supercell storm displaying the "flying eagle" or "v-notch" signature over north-central Kentucky on 28 May, 1996, observed with the National Weather Service WSR-88D radar compared to a flying bald eagle. Adapted from the National Weather Service WFO in Louisville, Kentucky (NWS Louisville, 2008).

In this paper we will provide a brief overview of previous studies that mention the flying eagle signature and why we feel that uncertainty exists even today. Next we present a condensed version of the linear theory analysis (e.g., Rotunno and Klemp 1982) that provides a better interpretation of this feature. Data from observations and numerical modeling are presented and compared to the linear theory. Finally, a discussion of any microphysical differences in the wings revealed from polarimetric radar and any operational merit of the flying eagle is presented.

**Corresponding author address*: Matthew Kumjian, 120 David L. Boren Blvd, National Weather Center Suite 4900, Norman, OK 73072. Email: matthew.kumjian@noaa.gov

2. HISTORY

Numerous early studies of severe storms were concerned with the airflow patterns in and around the convective cloud. Many of these investigators suggested that the midlevel and upper-level flow pattern around a convective tower was analogous to flow around a cylindrical obstacle (e.g., Newton and Newton 1959; Fujita 1965; Fankhauser 1971; Brown 1992). It was claimed that such blocking caused eddies to form in the lee of the tower (e.g., Jessup 1972). Hitschfeld (1960) used the analogy of a solid cylinder in the flow despite the fact that he admitted it was not the best analogy, just that it was the best available explanation at the time.

Despite the uncertainty in explanation and interpretation, some noted the v-notch signature's usefulness in diagnosing potentially severe storms (Lemon 1980). In fact, operational meteorologists in the pre-Doppler era had noted that such a feature on their radar displays was a useful indicator of strong storms (see Whiton et al. 1998). Additionally, a similar feature in satellite data was explored, providing forecasters additional information about developing convection with powerful updrafts (McCann 1983).

Later theoretical considerations (e.g., Rotunno 1981) demonstrated the flaws in the obstacle-flow analogy. Early numerical models also demonstrated that pressure distributions around the convective tower looked quite different than what one would expect from a solid obstacle, while also being able to reproduce the signature to some degree (Rotunno and Klemp 1982). The aforementioned studies invoked a linearization of the Boussinesq inviscid equations of motion, from which it can be shown the distribution of pressure perturbations arising from environmental wind shear interacting with an updraft. This is discussed further in the next section.

The motivation for this study comes in part from the uncertainty about the origins of this radar feature evident even today. For example, a recently-published paper remarks that the origin of the winged appearance in the reflectivity field "remains unknown" (Van Den Broeke et al. 2008). Another paper currently in press (Frame et al. 2009) analyzes radar data from a weak supercell that displays a particularly good example of the winged reflectivity field. However, they only conclude that neither size sorting nor storm splitting was "responsible for the maintenance of the prominent" signature without providing an interpretation (or how

they reached this conclusion). When discussing the flying eagle with various members of the weather community, we often find meteorologists misattributing the signature to obstacle flow around the updraft (even on a NWS WFO training website!). Additionally, to the authors' knowledge there is no thorough documentation of the signature, its origin, and its interpretation found in the literature with the exception of the training materials based on Lemon (1980), who first identified the signature on radar displays and realized its value to forecasters as an indication of severe weather. Thus, this paper aims to clear up some existing confusion about the signature as well as shed some new insight into its possible interpretation, importance, and microphysical characteristics. We will start by reviewing the well-known linear theory in the following section (Section 3). Next, output from numerical simulations of supercells is presented in Section 4. Observations of the signature from the research prototype polarimetric WSR-88D radar (KOUN) are provided in Section 5. Section 6 briefly summarizes the main conclusions of the paper.

3. LINEAR THEORY

For the interpretation of the dynamics of deep convection, we will follow tradition and consider the Boussinesq inviscid equations of motion (ignoring Coriolis effects):

$$\frac{D\vec{\mathbf{v}}}{Dt} = \frac{\partial \vec{\mathbf{v}}}{\partial t} + \left(\vec{\mathbf{v}} \bullet \nabla\right)\vec{\mathbf{v}} = -\frac{1}{\rho_0}\nabla p' + B\hat{\mathbf{k}} \qquad (1)$$

After taking the divergence of equation (1), we form a Poisson equation for p' which can be expressed in terms of physical quantities like three-dimensional deformation $\vec{\mathbf{D}}$ and three-dimensional vorticity $\vec{\omega}$

$$\frac{1}{\rho_0}\nabla^2 p' = -\left[\left(\frac{\partial u}{\partial x}\right)^2 + \left(\frac{\partial v}{\partial y}\right)^2 + \left(\frac{\partial w}{\partial z}\right)^2\right] - \frac{1}{2}\left|\vec{\mathbf{D}}\right| + \frac{1}{2}\left|\vec{\omega}\right| + \frac{\partial B}{\partial z} \qquad (2)$$

Following Rotunno and Klemp (1982), we then linearize (2) about a base state in which the horizontal wind is a function of height only $\vec{\mathbf{V}}$ = (U, V) and the vertical wind is zero (perturbations on all three components of the wind vary in space and time), and neglect fluid extension terms, horizontal vorticity, and deformation,

$$\frac{1}{\rho_0}\nabla^2 p' = \frac{1}{2}\left|\zeta'\right|^2 + \frac{\partial B}{\partial z} - 2\left(\frac{D\vec{\mathbf{V}}}{Dz} \bullet \nabla w'\right) \qquad (3)$$

The last term on the right hand side of (3) is the linear shear term that depicts the pressure perturbation associated with vertical wind shear interacting with an updraft. Using the assumption that the Laplacian of p' ~ - p', it follows that a positive pressure perturbation is located on the upshear side of the updraft and a negative pressure perturbation is located on the downshear side of the updraft. It is important to note that the upshear (downshear) side does not necessarily correspond to the upwind (downwind) side of the updraft, especially in environments in which winds veer with height.

It is this shear-induced perturbation pressure that acts to deflect the flow as it approaches the updraft. This is not to say that the flow does not penetrate the updraft; since the updraft is fluid it is porous to parcels in the environmental flow. However, these shear-induced pressure perturbations do influence the flow by deflecting it in and around the updraft. Thermodynamic observations within updrafts tend to show that the mixing of environmental air is confined to the edges (e.g., Bluestein and Gaddy 2001). Hydrometeors falling from the storm summit will be advected by this modified flow pattern.

4. NUMERICAL SIMULATIONS

4.1. Model Setup

The Advanced Regional Prediction System (ARPS) is used to simulate the Del City, Oklahoma tornadic supercell of 20 May 1977. Details of the ARPS model can be found in Xue et al. (1995). The simulation is initialized with a smoothed sounding from Klemp et al. (1981) and Xue et al. (2001). The storm is initiated by an ellipsoidal thermal bubble (+4 K perturbation) centered at a height of 1.5 km AGL, with the environment characterized by the sounding in Figure 2. The horizontal grid spacing is 1 km, and the vertical mesh is stretched from 100-m resolution near the ground to 700 m near the top of the domain, which is 64 km x 64 km x 16 km. Kessler (1969)-type warm rain microphysics is used. A fourth-order centered leap-frog scheme is used to advect the momentum fields. Additional details of the model parameters and schemes can be found in Xue et al. (2001).

4.2. Experiments

The first experiment is identical to that run by Xue et al. (2001). Early into the storm life cycle, a v-notch

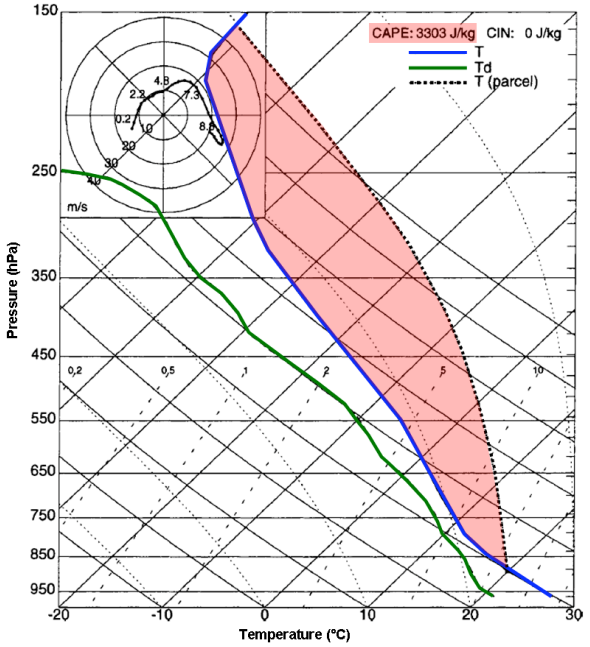

Fig. 2: Sounding and hodograph used to initialize the model: a smoothed version of the sounding on 20 May 1977. The blue line is the temperature, the green line is the dewpoint temperature, the black dotted line is the parcel temperature, and the shaded red area indicates the CAPE. Adapted from Xue et al. (2001).

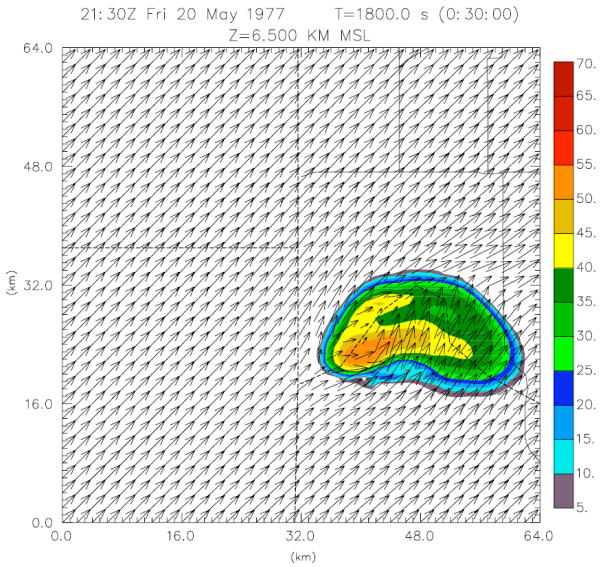

Fig. 3: Simulated radar reflectivity from 30 minutes into the simulation, at 6.5 km AGL. The horizontal wind vectors are overlaid. The reflectivity color scale is given in dBZ to the right of the image

or flying eagle signature is apparent in the simulated midlevel radar reflectivity field (Fig. 3). To investigate the cause of this signature, the pressure perturbation field from the same time and height is given in Figure 4, along with streamlines of the horizontal flow and contoured vertical velocities. The maximum updraft speed at this level is approximately 20 m s^{-1}. Clearly, a positive pressure perturbation is located on the western edge of the updraft, while a stronger negative pressure perturbation is located on the right edge of the updraft. The maximum pressure perturbation (1.2 hPa) is only about half the magnitude of the minimum pressure perturbation (-2.2 hPa), which is likely enhanced by buoyancy-related effects due to the warm updraft and by the pressure decrease associated with the cyclonic vorticity found on this flank of the updraft (see equation 3). The streamlines show the flow diverging around the updraft, though one streamline does pass into the updraft, indicating that updraft is not impenetrable.

In the next experiment, the hodograph is multiplied by a factor of $2^{1/2}$, increasing the flow speed as well as the shear. A larger domain is used to keep the storm within view. This simulated storm has notable differences from the first experiment. First, the enhanced flow spreads the precipitation much farther downstream, elongating the precipitation fields (inferred from the simulated radar reflectivity). The updraft is also weaker in this simulation, likely a result of being somewhat inhibited by the stronger shear. Not surprisingly, the weaker updraft results in less precipitation being lofted, resulting in lower reflectivity values. A v-notch type signature does appear aloft, however (Fig. 5). Compared to the previous run, the wings extend much farther downstream, a result of the stronger flow. It is important to note that the image in Fig. 5 is from 60 minutes into the simulation, so it took twice as long for the signature to appear as shown. Figure 6 displays the pressure perturbations: the upshear side of the updraft has a maximum perturbation of 1.14 hPa, roughly the same as the previous case. However, the minimum perturbation is only -0.44 hPa, half an order of magnitude as in the previous case. This is likely due to the lack of contributions from the buoyant updraft and vertical vorticity. Note also that the streamlines are not deflected to the same extent as in the previous case.

4.3. Analysis of Results and Future Simulations

Despite weakening the updraft, the stronger flow produces a more prominent flying eagle precipitation field. We expect that a stronger updraft would enhance the magnitudes of the pressure perturbations, causing more of a deflection and perhaps spreading the wings farther apart. Further sensitivity tests are necessary to quantify the behavior of the flying eagle, including experiments that systematically alter not only the shear but also the updraft intensity. From the linear theory analysis in the previous section, it is obvious that both

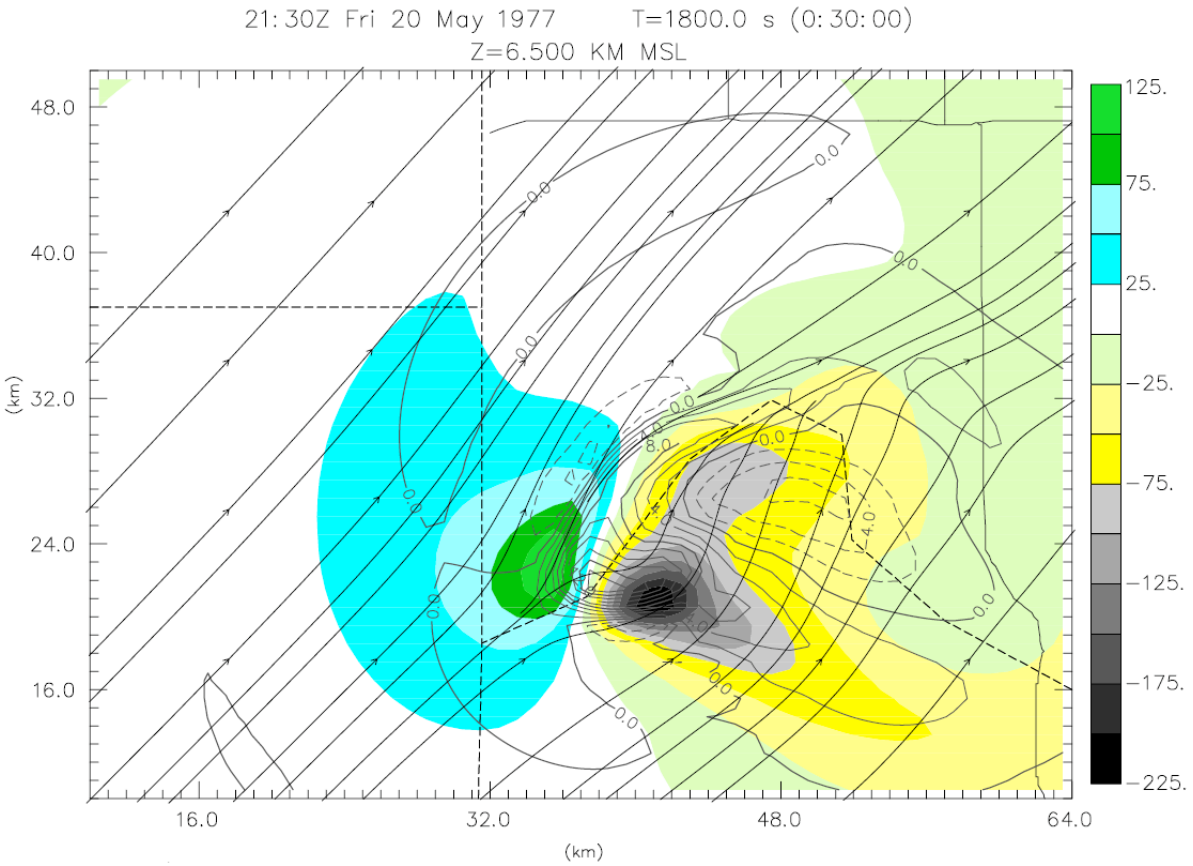

Fig. 4: From the same time and level as in the previous figure, but zoomed in on the storm. The colored shading represents the total pressure perturbation (in Pa). Overlaid are contours of vertical velocity and horizontal streamlines

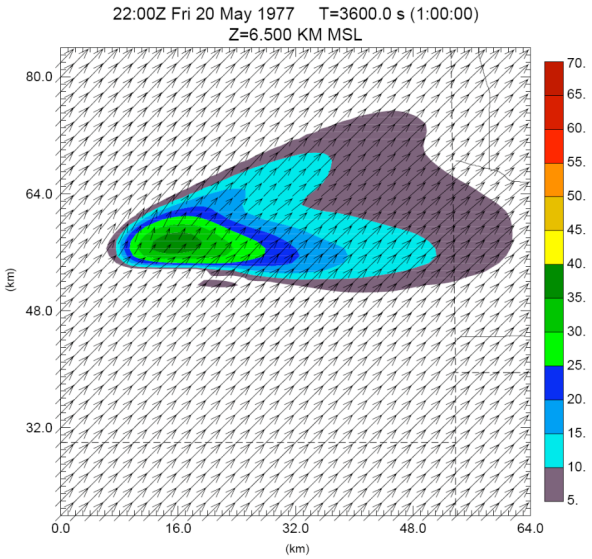

Fig. 5: As in Fig. 3, except for the second simulation at 60 minutes into the simulation.

updraft strength and the strength of the flow have an effect on the signature's appearance. The two simulations above suggest that the environmental flow is the dominant factor, though it is impossible to make any generalizations from such a small number of experiments. Interestingly, the relative weakness of the pressure perturbations in the second experiment (and consequent lack of streamline deflection) still results in a v-notch signature. One must consider not just the flow at levels where the signature is present, but the distribution of precipitation and the flow pattern aloft.

A warm rain microphysics parameterization was employed in the experiments above. Obviously, warm rain microphysics oversimplifies the nature of convective storms. We selected warm rain microphysics for computational efficiency, though ice microphysics parameterizations should be used in the future. We expect that the inclusion of ice hydrometeors would enhance the signature. This is because ice hydrometeors (with the exception of hail or large graupel) tend to fall slower than raindrops of comparable mass. The inclusion of ice would allow storm-top divergence to spread hydrometeors farther, allowing them to be advected farther downstream by

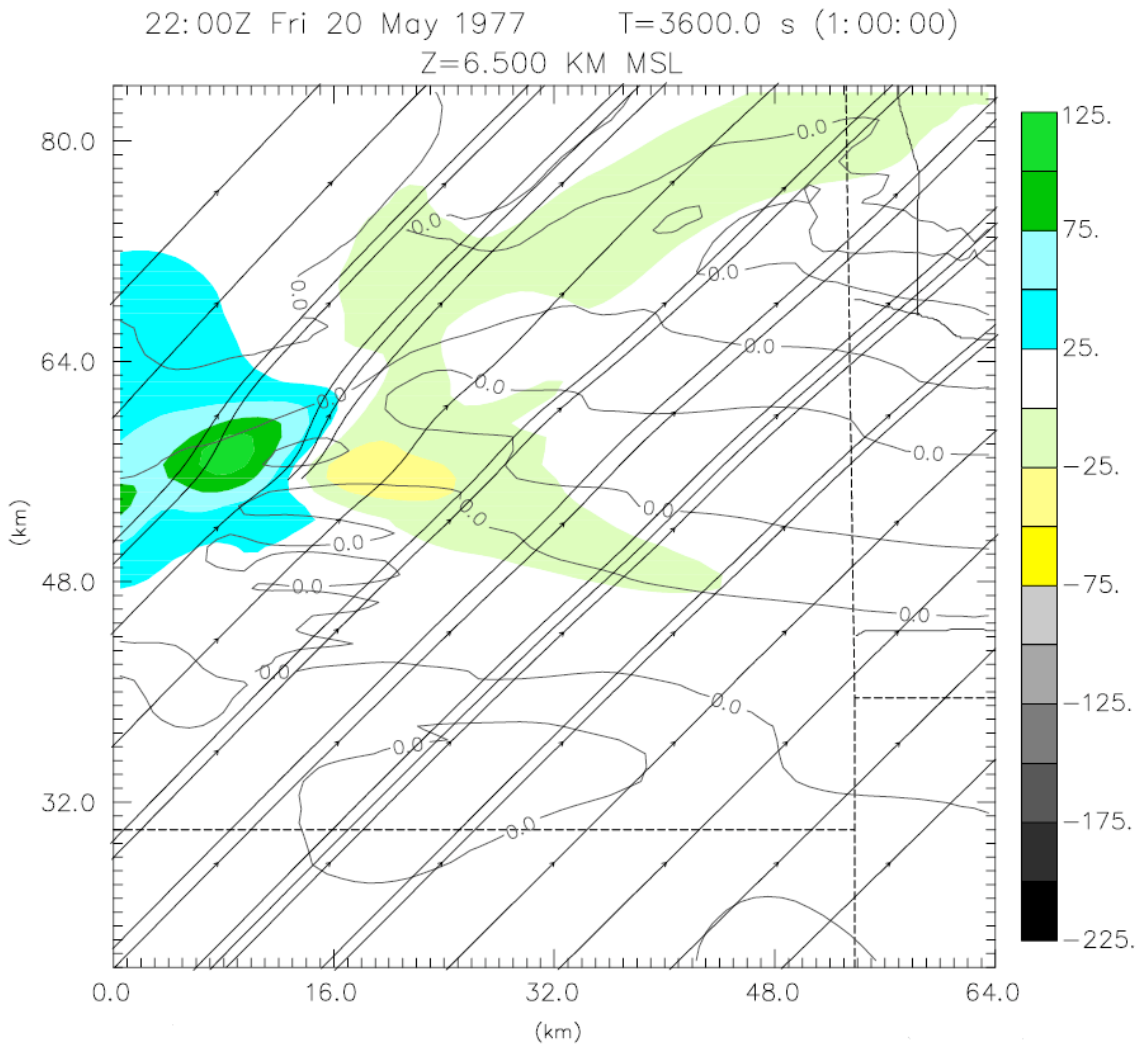

Fig. 6: As in Fig. 4, but for the second simulation.

the modified flow, resulting in a more prominent flying eagle signature. The next section will discuss the microphysics in more detail, supplemented with polarimetric radar observations.

5. POLARIMETRIC RADAR OBSERVATIONS – MICROPHYSICS

In a cursory look at the polarimetric dataset of supercell storms, it is evident that the flying eagle signature is present at some point in the lifetime of most storms. The prominence and persistence of the signature varies widely from storm to storm, however. There exists some evidence that the signature is more prominent as the storm begins to occlude, in both tornadic and nontornadic storms. This is not in contradiction of Van Den Broeke et al. (2008), who found that the signature is most likely at times leading to tornadogenesis in the sample of tornadic storms they investigated. However, our dataset includes numerous nontornadic supercells.

Microphysically, each wing tends to be somewhat similar, though in some cases subtle differences exist. In general, the northern (left) wing consists of mainly rain, as deduced from the polarimetric variables. The southern (right) wing extends from the hail core, and thus sometimes hail or melting hail and graupel are present in this branch. In general, the southern wing has higher Z_H, Z_{DR}, K_{DP}, and lower ρ_{HV} than the northern branch. It is possible that the southern wing's closer proximity to the main updraft explains the greater likelihood of hail being found in this region. A schematic of the distribution of hydrometeor species at low levels summarizes this difference (Fig. 7).

The largest hail remains in the core just to the north of the updraft. For such large hail to form, prolonged residence time in the updraft is evidently required (e.g., Miller et al. 1988). Lofted hailstones within the upper

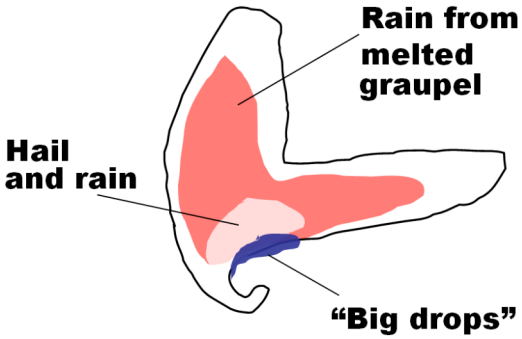

Fig. 7: Schematic showing the distribution of hydrometeors at low levels of a supercell storm displaying the flying eagle signature. The black outline represents the ~35 dBZ contour. Red shading indicates heavy rain from melted graupel and hail, the white shading indicates the hail core (generally mixed with rain), and the blue shading indicates the region of large drops known as the Z_{DR} arc. Farther out in the wings, light to moderate rain comes from melted snow and other small ice particles.

portions of the updraft can sometimes cause a marked decrease in ρ_{HV} (Kumjian and Ryzhkov 2008), analogous to a "cap" of higher LDR values (Hubbert et al. 1998) described in some previous studies. Since the updraft signature is usually confined to small region, we do not expect these hailstones to be responsible for rain in the wings. This is because such large hailstones have very large terminal velocities and thus will not be advected very far in their descent to the surface, confining them to regions close to the updraft. Thus, we should not expect large hail in the downstream portions of the wings.

It is important to note that the precipitation echo for such supercell storms tends to become circular with increasing height. In another word, the wings disappear as the radar observes the storm near the updraft summit. Atop the updraft, polarimetric data often indicate a broad region of graupel surrounded by snowflakes. The divergence at the storm summit is probably responsible for distributing precipitation particles quasi-uniformly. As these ice hydrometeors fall and are advected by the prevailing winds (which have been modified by the presence of the updraft) they are distributed into increasingly separate wings, where they eventually melt. Note that on the southern flank of the storm, the intense storm inflow at low levels likely recirculates or "recycles" some of these hydrometeors into the updraft, as suggested by Conway and Zrnić (1993). This may be responsible for the decreased areal extent of the southern wing in some cases.

6. CONCLUSIONS

In this paper we attempt to clarify several aspects of the flying eagle or v-notch radar signature often observed in supercell storms. Linear theory is invoked to describe the pressure perturbations associated with a convective updraft in the presence of vertical shear. It appears then that the signature (to some extent) should be a function of the strength of the middle and upper level flow and vertical shear as well as the strength of the updraft. The upshear pressure perturbation appears to be an important factor for deflecting the streamlines to the left, around the updraft. As exhibited in equation (3), stronger vertical shear and/or updraft will be associated with a larger pressure perturbation, resulting in a larger deflection of the flow. Further studies employing numerical models like the one utilized in section 4 may help quantify the sensitivity of the flying eagle signature's appearance to the strength of vertical shear, the updraft, and other factors. Polarimetric measurements illuminate subtle microphysical differences in the wings of the signature, elucidating the hydrometeor source regions to some extent.

The flying eagle signature is most commonly observed in supercells; in fact, to our knowledge, there are no known documented cases of nonsupercell storms that display such a signature. Perhaps, in accordance with linear theory, the signature requires a certain combination of vertical shear and updraft strength that characterize supercells and their environments but not ordinary convective storms. In other words, in the same way that supercell storms require particular environments to develop, the signature may also only develop if certain thresholds are attained. If it is true that only supercells display such a signature, then its appearance is a good indicator of supercell development. However, even weak and short-lived supercells display this signature on occasion, so it is unlikely that it is a direct measure of storm severity.

Despite the information gained by the theoretical, numerical, and observational techniques employed for this study, more questions persist. For instance, how important is the role of the pressure perturbations deflecting the flow relative to the strength of the mid- and upper-level flow? What is the operational merit of the signature? Do changes in the flying eagle correlate to significant events in the storm's evolution? Future work will hopefully begin to answer some of these questions.

7. REFERENCES

Bluestein, H.B. and S.G. Gaddy, 2001: Airborne pseudo-dual-Doppler analysis of a rear inflow jet and deep convergence zone within a supercell. *Mon. Wea. Rev.*, **129**, 2270-2289.

Brown, R. A., 1992: Initiation and evolution of updraft rotation within an incipient supercell thunderstorm. *J. Atmos. Sci.,* **49,** 1997–2014.

Conway, J.W. and D.S. Zrnić, 1993: A study of production and hail growth using dual-Doppler and multiparameter radars. *Mon. Wea. Rev.*, **121**, 2511-2528.

Fankhauser, J. C., 1971: Thunderstorm environment interactions determined from aircraft and radar observations. *Mon. Wea. Rev.,* **99,** 171–192.

Frame, J., P.M. Markowski, Y. Richardson, J.M. Straka, and J. Wurman, 2009: Polarimetric and dual-Doppler radar observations of the Lipscomb County, Texas supercell thunderstorm on 23 May 2002. *Mon. Wea. Rev.*, **in press.**

Fujita, T., 1965: Formation and steering mechanisms of tornado cyclones and associated hook echoes. *Mon. Wea. Rev.,* **93,** 67–78.

Hitschfeld, W., 1960: The motion and erosion of convective storms in severe vertical shear. *J. Atmos. Sci.*, **17**, 270–282.

Hubbert, J., V.N. Bringi, L.D. Carey, and S. Bolen, 1998: CSU-CHILL polarimetric measurements from a severe hailstorm in eastern Colorado. *J. Appl. Meteor.*, **37**, 749-755.

Jessup, E.A., 1972: Interpretations of chaff trajectories near a severe thunderstorm. *Mon. Wea. Rev.*, **100**, 653-661.

Kessler, E., 1969: On the distribution and continuity of water substance in atmospheric circulations, 84 pp.

Klemp, J.B., R.B. Wilhelmson, and P.S. Ray, 1981: Observed and numerically simulated structure of a mature supercell thunderstorm. *J. Atmos. Sci.*, **38**, 1558-1580.

Kumjian, M.R. and A.V. Ryzhkov, 2008: Polarimetric signatures in supercell thunderstorms. *J. Appl. Meteor. and Climatology*, **47**, 1940-1961.

Lemon, L. R., 1980: Severe thunderstorm radar identification techniques and warning criteria: A preliminary report. NOAA Tech. Memo. NWS NSSFC-1, 60 pp. [NTIS PB273049.]

McCann, D.W., 1983: The Enhanced-V: A satellite observable severe storm signature. *Mon. Wea. Rev.*, **111**, 887–894.

Miller, L.J., J.D. Tuttle, and C.A. Knight, 1988: Airflow and hail growth in a severe northern High Plains supercell. *J. Atmos. Sci.*, **45**, 736-762.

National Weather Service, Louisville, KY, 2008: Online informational page. Accessed October 2008: http://www.crh.noaa.gov/lmk/soo/docu/supercell.php

Newton, C. W., and H. R. Newton, 1959: Dynamical interactions between large convective clouds and environmental vertical shear. *J. Meteor.,* **16,** 483–496.

Rotunno, R., 1981: On the evolution of thunderstorm rotation. *Mon. Wea. Rev.,* **109,** 577–586.

Rotunno, R., and J. B. Klemp, 1982: The influence of the shear-induced pressure gradient on thunderstorm motion. *Mon. Wea. Rev.,* **110,** 136–151.

Van Den Broeke, M.S., J.M. Straka, and E.N. Rasmussen, 2008: Polarimetric radar observations at low levels during tornado life cycles in a small sample of classic southern plains supercells. *J. Appl. Meteor. and Climatology*, **47,** 1232-1247.

Whiton, R.C., P.L. Smith, S.G. Bigler, K.E. Wilk, and A.C. Harbuck, 1998: History of operational use of weather radar by U.S. Weather Services. Part I: The pre-NEXRAD era. *Wea. Forecasting*, **13**, 219–243.

Xue, M., K.K. Droegemeier, V. Wong, A. Shapiro, and K. Brewster, 1995: ARPS Version 4.0 User's Guide. Center for the Analysis and Prediction of Storms, [Available from CAPS, University of Oklahoma, Norman, OK 73072, 380 pp].

Xue, M., K.K. Droegemeier, V. Wong, A. Shapiro, K. Brewster, F. Carr, D. Weber, Y. Liu, and D. Wang, 2001: The Advanced Regional Prediction System (ARPS) – A multi-scale nonhydrostatic atmospheric simulation and prediction tool. Part II: Model physics and applications. *Meteorol. Atmos. Phys.*, **76**, 143-165.